JACS
JOURNAL OF THE AMERICAN CHEMICAL SOCIETY

Communication

pubs.acs.org/JACS

Electrochemically Driven Surface-Confined Acid/Base Reaction for an Ultrafast H^+ Supercapacitor

Shiyu Gan,[†] Lijie Zhong,[†,§] Lifang Gao,[†,‡] Dongxue Han,[†] and Li Niu*[,†]

[†]State Key Laboratory of Electroanalytical Chemistry, CAS Center for Excellence in Nanoscience, c/o Engineering Laboratory for Modern Analytical Techniques, Changchun Institute of Applied Chemistry, Chinese Academy of Sciences, Changchun 130022, China

[‡]University of Chinese Academy of Sciences, Beijing 100049, China

Supporting Information

ABSTRACT: We discovered an organic weak acid, 3,4,9,10-perylene tetracarboxylic acid (PTCA), confined on the electrode surface, revealing a reversible and ultrafast protonation/deprotonation non-Faradaic process but exhibiting analogous voltammetric peaks (capacitive peaks). A further synthesized PTCA−graphene supramolecular nanocomplex discloses a wide voltage window (1.2 V) and ultrahigh specific capacitance up to 143 F g^{-1} at an ultrafast charge−discharge density of 1000 A g^{-1} (at least 1 order of magnitude faster than present speeds). The capacitance retention maintained at 73% after 5000 cycles. This unique capacitive voltammetric behavior suggests a new type of charge-storage modes, which may offer a way for overcoming the present difficulties of supercapacitors.

Since the electric double layer (EDL) was inaugurated in the early 1900s, the EDL has been a fundamental model and theory to illustrate interfacial structures and electrochemical behaviors at electrode/electrolyte interfaces.[1] This theory unveils an analogous capacitor region existing at the nanoscale interface. However, this EDL capacitance is rather small (μF scale), far lower than the requirements for practical charge storage. Since the end of the last century, production of nanomaterials re-shed light on this field. Remarkable progress has been achieved, particularly for carbon-based and recently focused two-dimensional nanomaterials.[2−8] However, the charge-storage capacity remains a distance behind other energy storage devices. Another type is a pseudocapacitor that relies on an electron transfer (ET) Faradaic reaction for storing more charges.[2] However, similar to all Faradaic electrochemical systems, inherent overpotential limits the ultrafast charge−discharge ability. Current efforts are balancing the two considerations.

An electrochemically driven surface-confined acid/base reaction (protonation/deportonation) is a type of unique electrochemical reaction that was first reported by Smith and White in 1993.[9] They observed voltammetric peaks for self-assembled monolayers (SAM) of non-redox-active weak acids.[10] For example, Figure S1 shows cyclic voltammograms (CVs) and square voltammograms (SWVs) for an 11-mercaptoundecanoic acid (MUA) SAM on a polycrystal Au electrode similar to previous results on single-crystal Au electrodes.[11] It is interestingly found that a couple of CV peaks similar to a redox ET process appear but without any redox group in MUA. The same electrochemical behavior was observed in aromatic 4-mercaptobenzoic acid.[12] Early and recent theoretical studies demonstrate that these CV peaks originate from the electrochemically driven protonation/deprotonation at terminal carboxylic groups, which results in the change of interfacial differential capacitance (dC/dE is not a constant).[9,13−16] This unique electrochemical behavior cannot be attributed to EDL or the redox process (named "capacitive peak").

Along with this unique electrochemical behavior, we discovered a conjugated organic molecule, 3,4,9,10-perylene tetracarboxylic acid (PTCA), that exhibits the same electrochemically driven protonation/deprotonation behavior and importantly reveals ultrafast charge−discharge ability. This molecule is composed of a five-benzene core and four carboxylic groups at the edge (Figure 1a), which can be easily prepared by the hydrolysis of its anhydride. PTCA was directly deposited on the glassy carbon electrode (GCE). CVs reveal voltammetric peaks between −0.1 V and −0.6 V (vs SCE) in 1 M H_2SO_4 (Figure 1b). Although the benzene core has redox activity, it can only occur in the organic phase and at very negative potentials (−1.66 V vs SCE),[17] which was also supported by the control experiment of perylene without any voltammetric peak observed in aqueous solution (Figure S2b). Four split CV peaks in the potential negative-scan direction represent the four-step protonation process for the dissociated PTCA ($PTCA^{n-}$, n = 1−4). Peak 1 corresponds to the easiest protonation of $PTCA^{4-}$. It is observed that protonation peaks 1/2 and 3/4 have close potentials, indicating two equivalent positions of carboxylic groups (supported by the optimized molecular structure of PTCA, Figure S9g). Another characteristic is the increased current density from peak 1 to peak 4, which is consistent with the surface concentration distribution of $PTCA^{n-}$ determined by their pK_a. For example, the $PTCA^{4-}$ should have the lowest surface concentration, thus resulting in the lowest current response (peak 1). For the deprotonation, one strong peak at −0.35 V (overlapped 3/4 deprotonation) and one weak peak at −0.2 V (overlapped 1/2 deprotonation) are observed. These capacitive peaks show a linear relationship with the scan rate (inset of Figure 1b). The most important characteristic is ultrahigh scan rate endurance from 0.1 to 100 V s^{-1}, indicating ultrafast charge−discharge ability (Figure 1c and Figure S3).

Received: November 23, 2015
Published: January 21, 2016

DOI: 10.1021/jacs.5b12272
J. Am. Chem. Soc. 2016, 138, 1490−1493

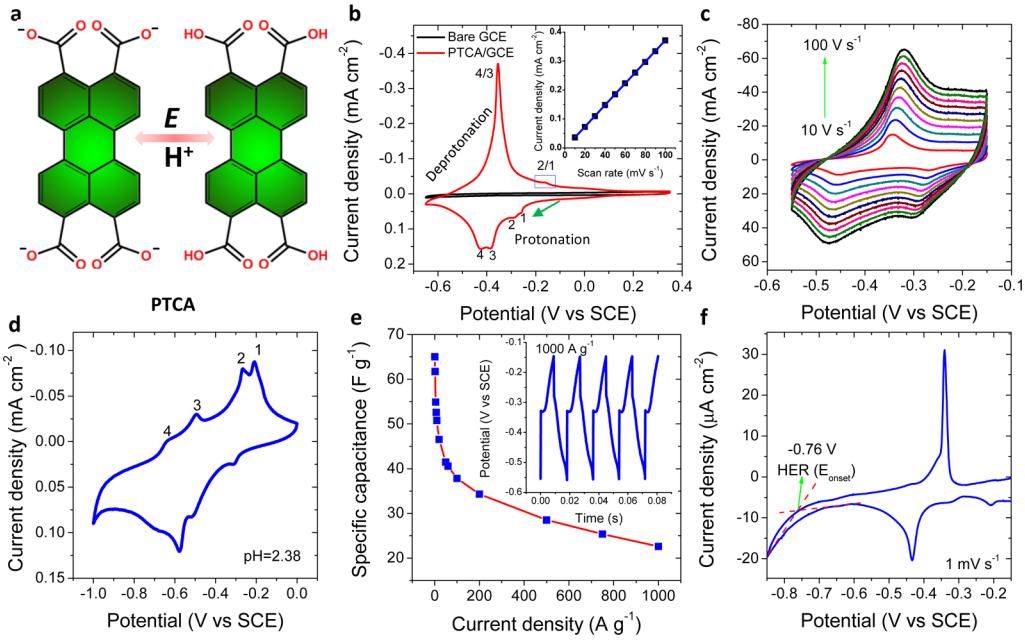

Figure 1. Electrochemically driven surface-confined acid/base reactions for PTCA. (a) Schematic illustration of the protonation/deprotonation process for PTCA driven by the electric field. (b) CV of PTCA/GCE and bare GCE in 1 M H_2SO_4. The magnified CV of bare GCE is shown in Figure S2a. The inset shows a linear relationship between current density of the selected deprotonation peak at −0.35 V (overlapped deprotonation peaks 4/3) and scan rates (10−100 mV s^{-1}). The arrow represents the scan direction from positive to negative potentials. (c) High scan rate CVs of PTCA/GCE from 10 to 100 V s^{-1} with IR compensation (2 Ω). Other CVs at 0.1−10 V s^{-1} are shown in Figure S3. (d) CVs of PTCA/GCE at pH 2.38 PBS solution. Scan rate: 100 mV s^{-1}. CVs at other pH solutions are shown in Figure S4. (e) Relationship between specific capacitance of PTCA and current density (1−1000 A g^{-1}). The inset shows a representative charge−discharge curve at 1000 A g^{-1}. (f) CV of PTCA/GCE in 1 M H_2SO_4 to examine the hydrogen evolution reaction.

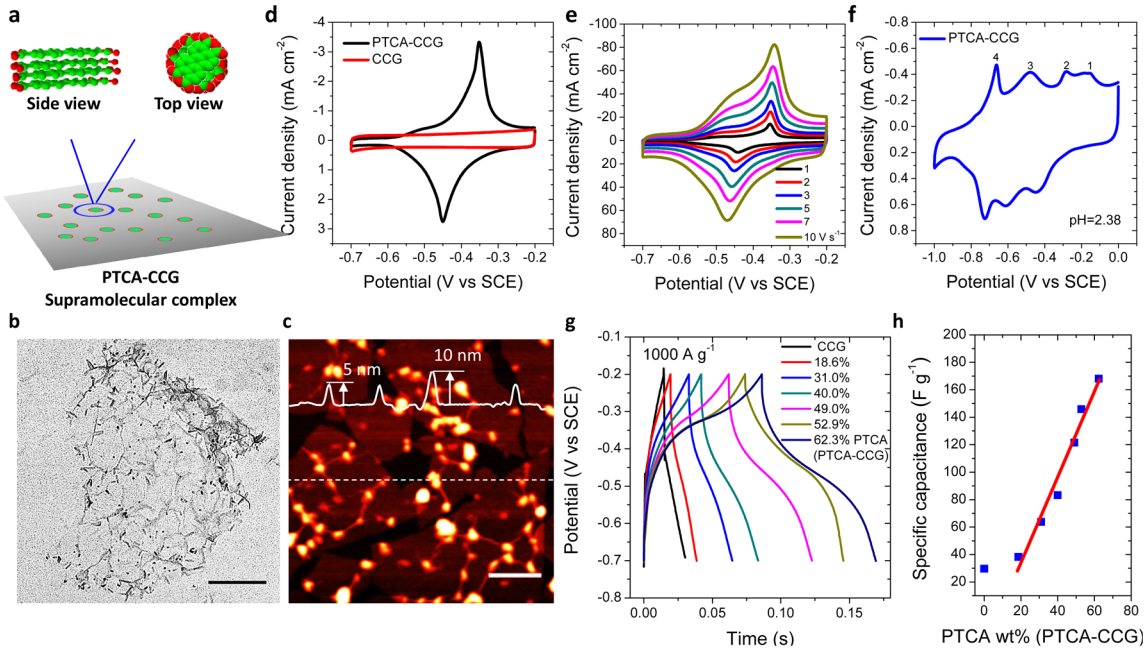

Figure 2. Electrochemical behavior of the PTCA−CCG supramolecular complex. (a) Schematic illustration of PTCA supramolecular self-assembly on CCG by π−π interactions. (b,c) Representative TEM and AFM images for PTCA−CCG, respectively. Scale bars: 300 nm. Corresponding thickness curve of PTCA−CCG was positioned on the AFM image along the marked line. (d) CVs of PTCA−CCG and CCG in 1 M H_2SO_4. Scan rate: 100 mV s^{-1}. (e) High scan rate CVs of PTCA−CCG from 1 to 10 V s^{-1} with IR compensation (2 Ω). (f) CV of PTCA−CCG in pH 2.38 PBS solution. Scan rate: 100 mV s^{-1}. CVs at other pH solutions are shown in Figure S11. (g) Charge−discharge curves for PTCA−CCG with varied PTCA weight content at high current density of 1000 A g^{-1}. (h) Relationship between specific capacitance at 1000 A g^{-1} and PTCA content.

It should be noted that the four protonation peaks are not always totally observed. It seems that they are sensitive to the surface state of the electrode and even scan rate. During 10 repeated experiments, the most observed cases are overlapped 1/2 protonation peaks (and/or 3/4 peaks). When the scan rate is high, overlapping is always observed. Moreover, peaks 1 and 2 are

DOI: 10.1021/jacs.5b12272
J. Am. Chem. Soc. 2016, 138, 1490−1493

sometimes very weak, but peaks 3 and 4 are always observed. We conjecture that it is related with the surface dissociate degree of PTCA in 1 M H_2SO_4. When the pH of the solution is gradually increased, we observed four well-defined peaks (Figure 1d). The pH-dependent protonation/deprotonation is shown in Figure S4. A linear correlation between peak potential of representative deprotonation peak 3 and pH is observed (Figure S4i). The determined slope (62 mV dec^{-1}) is very close to the previously reported MUA (67 mV dec^{-1}).[11] The discrepancy from theoretical 59 mV dec^{-1} might be attributed to the used applied electrode potential rather than more accurate local potential according to the Smith and White model.[9] In addition, we observed that the peak current decreases, and a few peaks disappear at higher pH, which indicates that PTCA dissolves gradually into the solution with the increase of the pH. The supercapacitor evaluation will be thus conducted in 1 M H_2SO_4. In addition, it was found that PTCA could strongly absorb on the surface of the GCE. The protonation/deprotonation peaks can still be observed even after the electrodes are polished, which can only be removed by sonication in NaOH solution (Figure S5). This phenomenon inspires us for the PTCA immobilized on graphene in the next discussion.

We further examine the charge−discharge ability of PTCA at high current densities from 1 to 1000 A g^{-1} (Figure 1e). PTCA shows ultrafast and reversible charge and discharge even at 1000 A g^{-1} (inset in Figure 1e and Figure S6). Corresponding specific capacitances are up to 65 and 23 F g^{-1} at 1 and 1000 A g^{-1}, respectively (Figure 1e). In addition, the interruption of the hydrogen evolution reaction (HER) was also examined. The onset potential of HER (E_{onset}) is determined at −0.76 V (Figure 1f), which is wider than the cutoff potentials for charge−discharge tests (−0.55 V for PTCA and −0.7 V for the following PTCA−CCG).

Inspired by the strong absorption ability of PTCA and structural similarity with chemically converted graphene (CCG), we prepared a PTCA−CCG supramolecular complex to further improve the specific capacitance performance based on graphene functionalization chemistry.[18,19] PTCA−CCG can be easily prepared by one-step reduction of a graphene oxide (GO)/PTCA mixture and purified by dialysis (Figure S7a). The fundamental material characterizations of PTCA−CCG are shown in Figure S8. For example, UV−vis absorption spectra of PTCA indicate remarkable red shifts after assembly on CCG (Figure S8a). Infrared spectra demonstrate reserved fingerprint information of PTCA on CCG (Figure S8b). X-ray diffraction confirms a weak crystalline structure of CCG dominating in the PTCA−CCG composite (Figure S8d). The $\pi-\pi$ interaction between the sp^2 plane of CCG and five-benzene core of PTCA causes the PTCA molecule to stack in a face-to-face mode on CCG and form hierarchical "nanobud-like" supramolecular nanostructures (Figure 2a−c and Figure S9). Compared with a thickness of 0.7 nm for the bare CCG, the thickness of the PTCA supramolecule is around 5−10 nm, indicating more than 15-layer stacking (0.34 nm for single PTCA molecule) (Figure 2c and Figure S9). The PTCA content (18.6−62.3%) on CCG can be controlled by adjusting its initial concentration ratio with GO.

The PTCA−CCG supramolecular complex exhibits electrochemical behaviors similar to those with pure PTCA. Main protonation/deprotonation peaks (3 and 4) at −0.45 V are observed (Figure 2d). It can also endure a high scan rate CV measurement (Figure 2e and Figure S10a). However, the current density (3.5 mA cm^{-2}) reveals 10-fold enhancements compared with that of pure PTCA (Figure 1b). It should be noted that the same loaded amounts of pure PTCA and PTCA−CCG were used for electrochemical tests. This remarkable enhancement indicates the active sites of the carboxylic group are sufficiently exposed, and the large surface area of CCG plays a key role. PTCA−CCG also shows no HER interruption in the potential window (Figure S10b). Analogously, all four peaks appear in pH 2.38 PBS solution (Figure 2f). The pH-dependent protonation/deprotonation behavior was also observed with a slope of 47 mV dec^{-1} (Figure S11). The specific capacitance increases by 2−9-fold compared with pure PTCA at 1000 A g^{-1} depending on the PTCA content (from 18.6 to 62.3%) (Figure 2g). Moreover, it is found that the specific capacitance exhibits a linear relationship with the PTCA content (Figure 2h).

Finally, we integrated PTCA−CCG into a prototype two-electrode setup for supercapacitor evaluation. As shown in Figures 1 and 2, the protonation/deprotonation behavior for PTCA and PTCA−CCG occurs at negative potentials. We have not yet found suitable positive electrode materials that disclose the same electrochemical characteristics. CCG was tried with a matched mass ratio to fabricate an asymmetric device. However, the assembled supercapacitor is quite unstable. To simplify this question, the carbon paper (CP) was used to offer sufficient positive electrode capacitance. Considering the lower electronic conductivity for higher PTCA content of PTCA−CCG, we did not use the as-prepared highest 62.3% PTCA−CCG while 52.9% PTCA−CCG was used as the negative electrode. The assembled PTCA−CCG/CP device reveals an enlarged potential window up to 1.2 V larger than 1 V for most carbon-based supercapacitors in aqueous solution (Figure 3a). Featured protonation/deprotonation CV peaks are observed at 0.4−1.2 V. PTCA−CCG also shows reversible charge−discharge curves, and the specific capacitances are 456, 235, 172, and 143 F g^{-1} at 1, 10,

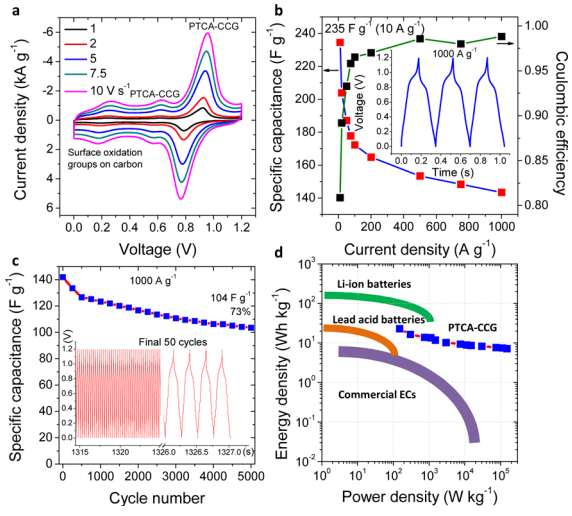

Figure 3. Supercapacitor performances of PTCA−CCG/CP in a prototype two-electrode setup. (a) High scan rate CVs of PTCA−CCG/CP in 1 M H_2SO_4 from 1 to 10 V s^{-1} with IR compensation (4.6 Ω). The PTCA content is 52.9% on PTCA-CCG. (b) Correlations between specific capacitance and Coulombic efficiency with current density. The inset shows representative charge−discharge curves at an ultrahigh current density of 1000 A g^{-1}. Other charge−discharge curves are shown in Figure S12. (c) Cyclic charge−discharge performance at 1000 A g^{-1} for 5000 cycles. The inset shows the final 50 cycles. (d) Ragone plots of specific energy density versus power density for PTCA−CCG in comparison with Li-ion batteries, lead-acid batteries, and commercial ECs.[2]

DOI: 10.1021/jacs.5b12272
J. Am. Chem. Soc. 2016, 138, 1490−1493

100, and 1000 A g^{-1} (Figure 3b, Figure S12, and Table S1). The highest Coulombic efficiency is 98% (Figure 3b), which is comparable to that of current EDL-based supercapacitors. After 5000 cycles at 1000 A g^{-1}, the capacitance retention is maintained at 73% (Figure 3c). The above measurements were performed in a low loading (0.034 mg cm^{-2}). We also examined the supercapacitor performances in a high loading (1 mg cm^{-2}). The main results are shown in Figure S13. The specific capacitance to a certain extent is reduced at high charge−discharge current densities, probably due to the IR drop effect. However, it remains at 309 and 230 F g^{-1} at 1 and 5 A g^{-1}, respectively (see more discussion in Figure S13). Compared with recently reported CCG-based supercapacitors, PTCA−CCG exhibits high gravimetric capacitance (Table S1). The energy/power density is even better than lead-acid batteries and commercial ECs (Figure 3d and Figure S13f). Although these initial results disclose promising performances, finding suitable positive electrode materials and establishing a full cell as well as macroscale devices should be crucial tasks in the near future.

Electrochemically driven protonation/deprotonation is a class of unique electrochemical processes.[10−12,20,21] The current standpoint is the change of interfacial capacitance upon ionization of surface groups. Intrinsic reasons, however, remain a complex question. A possible mechanism might be the structural conversion induced by ion association/disassociation, leading to remarkable changes of surface charges.[22] We finally try to offer our understanding in terms of soft-interface electrochemical views (Figure S14 and supporting discussion). There are, in fact, two types of charge transfers in electrochemical systems, ET and ion transfer (IT). At solid/liquid interfaces, ET is the only charge transfer mode because of the ion impermeability for the solid electrode. However, IT can occur at another electrochemical interface, such as a liquid/liquid interface (L/L, or soft interface), which constitutes immiscible biphasic systems (e.g., water/oil, Figure S14a). Both ET and IT processes can result in voltammetric peaks at soft interfaces.[23] We can consider the surface-confined PTCA as an individual phase analogous to the oil phase (Figure S14b). The H^+ transfer from water to PTCA is similar to that at the L/L interface. Due to the association with carboxylic groups, it can be further considered as facilitated H^+ transfer. Ultrafast charge/discharge ability for H^+ transfer between PTCA and water corresponds to a higher rate (1 order of magnitude) for IT than ET at the L/L interface.[24,25] Although the accurate mechanism needs further exploration, this unique electrochemical reaction offers a new charge-storage mode for supercapacitors.

The results reported herein highlight a classic electrochemical phenomenon, "electrochemically driven surface-confined acid/base reaction", for proposing a new type of ultrafast supercapacitors. The conjugated organic weak acid (PTCA) exhibits ultrafast charge−discharge ability. Another crucial step is the self-assembly of PTCA on CCG to form a supramolecular complex, which prominently enhances the energy density. These results might open a new branch for capacitor-based energy storage systems in addition to EDL and redox supercapacitors.

■ ASSOCIATED CONTENT

Supporting Information

The Supporting Information is available free of charge on the ACS Publications website at DOI: 10.1021/jacs.5b12272.

Experimental details, Figures S1−S14, and Table S1 (PDF)

■ AUTHOR INFORMATION

Corresponding Author

*lniu@ciac.ac.cn

Present Address

§Department of Energy Conversion and Storage, Technical University of Denmark, Kemitorvet Building 207, DK-2800 Kongens Lyngby, Denmark.

Notes

The authors declare no competing financial interest.

■ ACKNOWLEDGMENTS

This work was supported by the National Natural Science Foundation of China (Nos. 21505127, 21225524, 21175130, 21105096, and 21205112) and funds for the Construction of Taishan Scholars (No. ts201511058). We acknowledge the fruitful discussion with Jens Ulstrup, Qijin Chi, and Jingdong Zhang (Technical University of Denmark).

■ REFERENCES

(1) Parsons, R. *Chem. Rev.* **1990**, *90*, 813.
(2) Simon, P.; Gogotsi, Y. *Nat. Mater.* **2008**, *7*, 845.
(3) Simon, P.; Gogotsi, Y. *Acc. Chem. Res.* **2013**, *46*, 1094.
(4) Cui, C.; Qian, W.; Yu, Y.; Kong, C.; Yu, B.; Xiang, L.; Wei, F. *J. Am. Chem. Soc.* **2014**, *136*, 2256.
(5) Zhu, Y.; Murali, S.; Stoller, M. D.; Ganesh, K. J.; Cai, W.; Ferreira, P. J.; Pirkle, A.; Wallace, R. M.; Cychosz, K. A.; Thommes, M.; Su, D.; Stach, E. A.; Ruoff, R. S. *Science* **2011**, *332*, 1537.
(6) Yang, X.; Cheng, C.; Wang, Y.; Qiu, L.; Li, D. *Science* **2013**, *341*, 534.
(7) Liu, S.; Gordiichuk, P.; Wu, Z.-S.; Liu, Z.; Wei, W.; Wagner, M.; Mohamed-Noriega, N.; Wu, D.; Mai, Y.; Herrmann, A.; Mullen, K.; Feng, X. *Nat. Commun.* **2015**, *6*, 8817.
(8) Yang, Y.; Ruan, G.; Xiang, C.; Wang, G.; Tour, J. M. *J. Am. Chem. Soc.* **2014**, *136*, 6187.
(9) Smith, C. P.; White, H. S. *Langmuir* **1993**, *9*, 1.
(10) White, H. S.; Peterson, J. D.; Cui, Q. Z.; Stevenson, K. J. *J. Phys. Chem. B* **1998**, *102*, 2930.
(11) Burgess, I.; Seivewright, B.; Lennox, R. B. *Langmuir* **2006**, *22*, 4420.
(12) Rosendahl, S. M.; Burgess, I. J. *Electrochim. Acta* **2008**, *53*, 6759.
(13) Andreu, R.; Fawcett, W. R. *J. Phys. Chem.* **1994**, *98*, 12753.
(14) Fawcett, W. R.; Fedurco, M.; Kovacova, Z. *Langmuir* **1994**, *10*, 2403.
(15) Luque, A. M.; Mulder, W. H.; Calvente, J. J.; Cuesta, A.; Andreu, R. *Anal. Chem.* **2012**, *84*, 5778.
(16) Calvente, J. J.; Luque, A. M.; Andreu, R.; Mulder, W. H.; Olloqui-Sariego, J. L. *Anal. Chem.* **2013**, *85*, 4475.
(17) Parker, V. D. *J. Am. Chem. Soc.* **1976**, *98*, 98.
(18) Hirsch, A.; Englert, J. M.; Hauke, F. *Acc. Chem. Res.* **2013**, *46*, 87.
(19) Gan, S.; Zhong, L.; Engelbrekt, C.; Zhang, J.; Han, D.; Ulstrup, J.; Chi, Q.; Niu, L. *Nanoscale* **2014**, *6*, 10516.
(20) Chen, Y.; Yang, X.-J.; Jin, B.; Guo, L.-R.; Zheng, L.-M.; Xia, X.-H. *J. Phys. Chem. C* **2009**, *113*, 4515.
(21) Zhang, J. D.; Demetriou, A.; Welinder, A. C.; Albrecht, T.; Nichols, R. J.; Ulstrup, J. *Chem. Phys.* **2005**, *319*, 210.
(22) Magnussen, O. M. *Chem. Rev.* **2002**, *102*, 679.
(23) Samec, Z. *Pure Appl. Chem.* **2004**, *76*, 2147.
(24) Sun, P.; Li, F.; Chen, Y.; Zhang, M.; Zhang, Z.; Gao, Z.; Shao, Y. *J. Am. Chem. Soc.* **2003**, *125*, 9600.
(25) Liu, S.; Li, Q.; Shao, Y. *Chem. Soc. Rev.* **2011**, *40*, 2236.

DOI: 10.1021/jacs.5b12272
J. Am. Chem. Soc. 2016, 138, 1490−1493